Influence of iron on the elastic properties of wadsleyite and ringwoodite

M. Núñez-Valdez,[1] P. da Silveira,[2] and R. M. Wentzcovitch[3]

Received 19 March 2011; revised 6 October 2011; accepted 8 October 2011; published 28 December 2011.

[1] We investigate by first-principles the influence of iron on the elastic properties of the β–phase (wadsleyite) and γ–phase (ringwoodite), polymorphs of olivine, the most abundant minerals of the upper and lower parts of the transition zone, respectively. Our study aims to complement experiments to understand details of the 410 km and 520 km discontinuities. The full elastic-tensor C_{ij}, bulk (K), and shear (G) moduli are determined under static conditions for β–γ–$(Mg_{1-x}Fe_x)_2SiO_4$ with $x = 0.125$. Wave propagation anisotropy in single crystals and polarization anisotropy in aggregates with preferred orientation are investigated and compared with those of iron-free wadsleyite and ringwoodite for a thorough understanding of the effect of iron. We examine the effect of iron on velocity contrasts due to phase changes and conclude that iron enhances ΔV_P and ΔV_S across the $\alpha \rightarrow \beta$ transition but suppresses them across the $\beta \rightarrow \gamma$ transition. The latter might contribute to suppress locally the 520 km discontinuity if this has a significant contribution from the $\beta \rightarrow \gamma$ transition. We show that lateral variation of iron, δx, produces lateral velocity heterogeneity ratios similar to those produced by lateral variations of temperature, δT, both producing ratios comparable to values extracted from seismic tomography studies. However, in contrast with δT, δx produces negative values for density to longitudinal and shear wave velocity ratios. This might be considered the fingerprint of lateral variations of iron concentration. These negative ratios appear similar to results inferred from geodynamical models compiled by Karato and Karki (2001) for the upper mantle and transition zone.

Citation: Núñez-Valdez, M., P. da Silveira, and R. M. Wentzcovitch (2011), Influence of iron on the elastic properties of wadsleyite and ringwoodite, *J. Geophys. Res.*, *116*, B12207, doi:10.1029/2011JB008378.

1. Introduction

[2] Olivine (α–phase) and its high-pressure polymorphs, wadsleyite (β–phase) and ringwoodite (γ–phase), have chemical composition $(Mg_{1-x}Fe_x)_2SiO_4$ with $x \approx 0.1$, and are the most abundant minerals in the upper mantle [*Rinwood*, 1975; *Putnis*, 1992], and transition zone [*Irifune and Ringwood*, 1987]. Studies of their crystal chemistry, structure, and elasticity are important because of the association of pressure-induced phase transformations from olivine to wadsleyite ($\alpha \rightarrow \beta$) and from wadsleyite to ringwoodite ($\beta \rightarrow \gamma$) with the seismic wave velocity discontinuities near 410 and 520 km depth [*Revenaugh and Jordan*, 1991] in the Earth.

[3] Single-crystal elastic constants of β– and γ–$(Mg_{1-x}, Fe_x)_2SiO_4$ have been measured using Brillouin scattering for $x = 0$ at ambient conditions [*Sawamoto et al.*, 1984; *Weidner et al.*, 1984] and in the range of 0 to 14 GPa (β–phase) [*Zha et al.*, 1997]. There are also data for wadsleyite with $x = 0.08$ at ambient conditions and for ringwoodite with $x = 0.09$ in the 0–16 GPa interval [*Sinogeikin et al.*, 1998, 2003]. Ultrasonic interferometry techniques have been employed to measure sound velocities of polycrystalline aggregates of wadsleyite with $x = 0$ up to 12 GPa and $x = 0.12$ up to 9.6 GPa [*Li et al.*, 1996; *Li and Liebermann*, 2000]. There are also ultrasonic measurements of polycrystalline aggregates of ringwoodite with $x = 0$ up to 12 GPa and $x = 0.2$ up to 14 GPa [*Rigden et al.*, 1991; *Li*, 2003; *Higo et al.*, 2006]. However, ultrasonic interferometry results do not help in the interpretation of seismic anisotropy. On the other hand, first-principles elasticity is only available for the iron-free wadsleyite [*Kiefer et al.*, 2001] and ringwoodite [*Kiefer et al.*, 1997, 1999; *Panero*, 2008]. To address the 410 and 520 km discontinuities, researchers compare velocities obtained from theoretical and experimental elastic properties of these, and often coexisting, phases with changes in velocities from seismic data. From these comparisons the olivine content in the mantle can be inferred [*Sawamoto et al.*, 1984; *Zha et al.*, 1998; *Yu and Wentzcovitch*, 2006; *Li and Liebermann*, 2007; *Bass et al.*, 2008]. However,

[1]School of Physics and Astronomy, University of Minnesota, Minneapolis, Minnesota, USA.
[2]Scientific Computation Program, University of Minnesota, Minneapolis, Minnesota, USA.
[3]Department of Chemical Engineering and Materials Science, Minnesota Supercomputing Institute, University of Minnesota, Minneapolis, Minnesota, USA.

0148-0227/11/2011JB008378

Table 1. Unit Cell Volumes of Wadsleyite and Ringwoodite at Zero Pressure

β–$(Mg_{1-x},Fe_x)_2SiO_4$				γ–$(Mg_{1-x},Fe_x)_2SiO_4$			
Experiment	x	First Principles	x	Experiment	x	First Principles	x
535.30(27)[a]	0	530.80[b]	0	525.30(21)[c]	0	517.68[b]	0
535.8(2)[d]	0	527.4[e]	0	526.7(3)[f]	0	497.0[g]	0
539.26(4)[h]	0					514.0[i]	0
538.36(19)[a]	0.08	532.95[b]	0.125	526.2(4)[j]	0.09	519.94[b]	0.125
540.38(15)[a]	0.16						
539.4(4)[j]	0.08						

[a] *Hazen et al.* [1990].
[b] This work.
[c] *Weidner et al.* [1984].
[d] *Zha et al.* [1997].
[e] *Kiefer et al.* [2001].
[f] *Meng et al.* [1994].
[g] *Kiefer et al.* [1999].
[h] *Hazen et al.* [2000].
[i] *Panero* [2008].
[j] *Sinogeikin et al.* [1998].

owing to the lack of data on the elasticity of the iron-bearing β–γ–phases at pressures characteristic of the transition zone (~13.5–23 GPa), constraints in the amount of olivine rely on pure Mg end-members [*Yu et al.*, 2008] and/or large extrapolations from lower pressures.

[4] This study complements and extends investigations of elasticity of wadsleyite and ringwoodite by addressing the effect of iron. Previous work on the α–phase (olivine) [*Núñez Valdez et al.*, 2010], as well as perovskite and postperovskite [*Kiefer et al.*, 2002; *Hsu et al.*, 2011; *Caracas and Cohen*, 2008], have established the feasibility of using standard first-principles density functional theory to predict the elasticity of iron-bearing minerals with nonmetallic ground states. We present here first-principles static predictions of structure, equation of state, full elastic constant tensor C_{ij} of β– and γ–$(Mg_{1-x},Fe_x)_2SiO_4$ for $x = 0$ and $x = 0.125$ between 0 and 30 GPa, a range that encompasses transition zone pressures. Using these elastic tensors we calculate acoustic velocities, anisotropy in single crystals, and in fully isotropic and transversely isotropic aggregates. We also investigate velocity anomalies produced by structural phase transitions and velocity changes at constant pressure produced by variations in iron content (lateral variations).

2. Computational Methods

[5] Our first-principles study makes use of density functional theory (DFT) [*Hohenberg and Kohn*, 1964; *Kohn and Sham*, 1965], as implemented in the quantum-ESPRESSO code [*Giannozzi et al.*, 2009]. Then two major approximations are adopted: (1) electrons are treated within the Local Density Approximation (LDA) for the exchange-correlation energy functional [*Ceperley and Alder*, 1980] and (2) pseudopotentials for Fe, Si, and O were generated by the Vanderbilt method [*Vanderbilt*, 1990] and the pseudopotential for Mg was generated by the von Barth-Car method. The valance electronic configurations used are $3s^2 3p^6 3d^{6.5} 4s^1 4p^0$, $3s^2 3p^1$, and $2s^2 2p^4$ for Fe, Si, and O, respectively. Core radii for all quantum numbers l are 1.8 a.u. for Fe, 1.6 a.u. for Si, and 1.4 a.u. for O. The pseudopotential for Mg used five valance electronic configurations, $3s^2 3p^0$, $3s^1 3p^1$, $3s^1 3p^{0.5} 3\ d^{0.5}$, $3s^1 3p^{0.5}$, and $3s^1 3d^1$ with decreasing weights 1.5, 0.6, 0.3, 0.3, and 0.2, respectively. Core radii for all quantum numbers l are 2.5 a.u. The plane wave kinetic energy cutoff was chosen to be 40 Ry and for the charge density 160 Ry. $2 \times 2 \times 2$ and $4 \times 4 \times 4$ k-point meshes are used for the Brillouin zone sampling of wadsleyite and ringwoodite, respectively. Convergence tests in k-point meshes and energy cutoffs were performed and our final choices for this paper correspond to having interatomic forces smaller than 10^{-4} Ry/a.u. and pressure convergence within 0.5 GPa. In all situations investigated, β– and γ–phases were insulating.

[6] In order to obtain the ground state atomic configurations in equilibrium, cell shape and internal structural parameters were optimized under static conditions (0 K) at eight arbitrary pressures using a variable-cell-shape molecular dynamics technique [*Wentzcovitch*, 1991; *Wentzcovitch et al.*, 1993]. Throughout the pressure range of 0 to 30 GPa, the total electronic spin, which was free to vary during calculations, of Fe-bearing wadsleyite and ringwoodite was $S = 2$ and $S = 4$, namely, the high spin state.

[7] Wadsleyite, the β–phase of $(Mg_{1-x},Fe_x)_2SiO_4$, crystalizes in body centered orthorhombic symmetry corresponding to the space group *Imma*. Fe and Mg are distributed among three independent octahedral sites M1, M2, and M3 (4a, 4e, and 8g, respectively), Si is in the tetrahedral site T (8 h), and O occupies four positions O1, O2, O3, and O4 (4e, 4e, 8h, and 16j, respectively) [*Horiuchi and Sawamoto*, 1981; *Hazen et al.*, 1990]. In our calculations we use the primitive cell, with $Z = 4$ units, i.e., 28 atoms. The iron substitution considered is Fe → M1, iron in sites M2 or M3 was energetically less favorable than in M1 being M1 ≈ M3 < M2, this is also consistent with experimental data [*Finger et al.*, 1993]. Moreover in the study of olivine [*Núñez Valdez et al.*, 2010], the two octahedral sites were tested for iron substitution and the results indicated a difference between the single-crystal elastic constants of Fe → M1 and Fe → M2 of less than 4% in average. Aggregate properties (bulk and shear moduli) were basically unaffected by the choice of octahedral site for Fe.

[8] Ringwoodite, the γ–phase of $(Mg_{1-x},Fe_x)_2SiO_4$, has a spinel face centered cubic structure (space group $Fd\bar{3}m$)

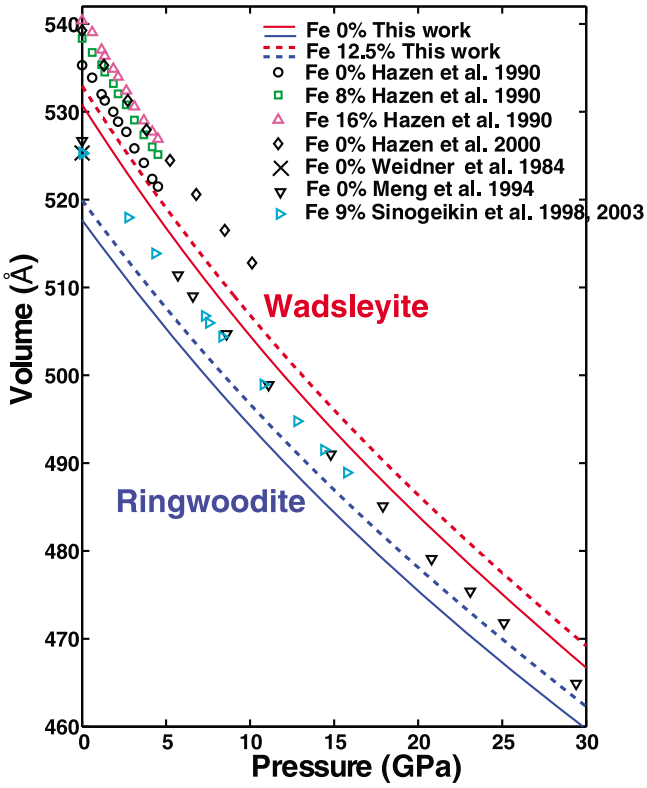

Figure 1. Static equations of state of wadsleyite and ringwoodite compared with experimental measurements at room temperature.

with the Fe and Mg ions occupying octahedral interstitial sites (16d). Si occupies interstitial tetrahedral sites (8a) and O (32e) forming isolated SiO_4 tetrahedra [*Finger et al.*, 1979]. The unit cell has $Z = 8$ units equivalent to 56 atoms. Calculations of the elasticity of ringwoodite were performed using this unit cell. To account for $x = 0.125$, two Fe atoms, with one iron at the center of the cell, were placed with a separation that was neither the largest nor the shortest. The choice of octahedral site and its effects, as mentioned above, were studied for olivine [*Núñez Valdez et al.*, 2010].

[9] To obtain the elastic constants C_{ij} (in Voigt notation [*Wallace*, 1972]) at each pressure, the equilibrium structures were strained, and their internal degrees of freedom re-relaxed. Using the stress–strain relationship:

$$\sigma_{ij} = C_{ijkl}\varepsilon_{kl}, \tag{1}$$

positive and negative strains of 1% magnitude were applied in order to attain accuracy in the limit of zero strain. The theoretical handling of C_{ij} is described by *Núñez Valdez et al.* [2010] and the general method has been applied to other solids and minerals for over a decade [*Wentzcovitch et al.*, 1995; *Karki et al.*, 1997]. All calculations reported here were obtained using the C_{ij} workflow as implemented in the VLab cyberinfrastructure [*da Silveira et al.*, 2008].

3. Results

3.1. Equation of State

[10] Upon substitution of one Mg atom by one Fe ($x = 0.125$), wadsleyite lattice parameters **a** and **c** increase by ~0.46% and ~0.12%, respectively, while **b** decreases by ~0.1%. These results are in agreement with experimental data by *Finger et al.* [1993] and *Hazen et al.* [2000]. The increase in volume of wadsleyite at 0 GPa is ~0.4%. In ringwoodite the volume increases by ~0.45%; thus the equation of state of the γ–phase is slightly more affected by iron than that of the β–phase (see Table 1 and Figure 1). As it is well known, the static LDA method tends to underestimate the volume. For β–Mg_2SiO_4, the predicted zero-pressure lattice parameters are $a = 5.6862$ Å, $b = 11.3902$ Å, and $c = 8.1939$ Å, which yield a volume smaller by ~1% with respect to results by *Hazen et al.* [1990] of $a = 5.6810(28)$ Å, $b = 11.4406(8)$ Å, and $c = 8.2361(7)$ Å. For γ–Mg_2SiO_4, our predicted volume is ~1.5% with $a = 8.0292$ Å compared to the volume reported by *Weidner et al.* [1984], $a = 8.0687(7)$ Å, at ambient conditions.

Table 2. First Principles Elastic Moduli C_{ij} (GPa)

P	x	C_{11}	C_{22}	C_{33}	C_{44}	C_{55}	C_{66}	C_{12}	C_{13}	C_{23}
					β–$(Mg_{1-x},Fe_x)_2SiO_4$					
0[a]	0	369.5	366.4	283.3	103.6	115.1	106.7	85.3	100.6	106.5
0[b]	*0*	*377*	*375*	*294*	*108*	*117*	*109*	*90*	*102*	*107*
0[a]	0.125	364.3	358.7	278.5	100.8	103.5	100.0	96.8	110.0	109.5
30[a]	0	530.8	516.6	440.4	121.3	132.2	147.8	195.2	192.3	213.5
30[a]	0.125	522.4	504.5	438.3	114.2	115.7	142.5	212.0	201.6	216.6
					γ–$(Mg_{1-x},Fe_x)_2SiO_4$					
0[a]	0	351.0			130.7			119.3		
0[c]	*0*	*361*			*134*			*118*		
0[d]	*0*	*358.3*			*133.5*			*117.9*		
0[a]	0.125	345.8			126.9			123.4		
30[a]	0	510.4			148.9			220.4		
30[a]	0.125	506.0			138.9			226.1		

[a]This work at pressures $P = 0$ and 30 GPa.
[b]*Kiefer et al.* [2001].
[c]*Kiefer et al.* [1997].
[d]*Panero* [2008].

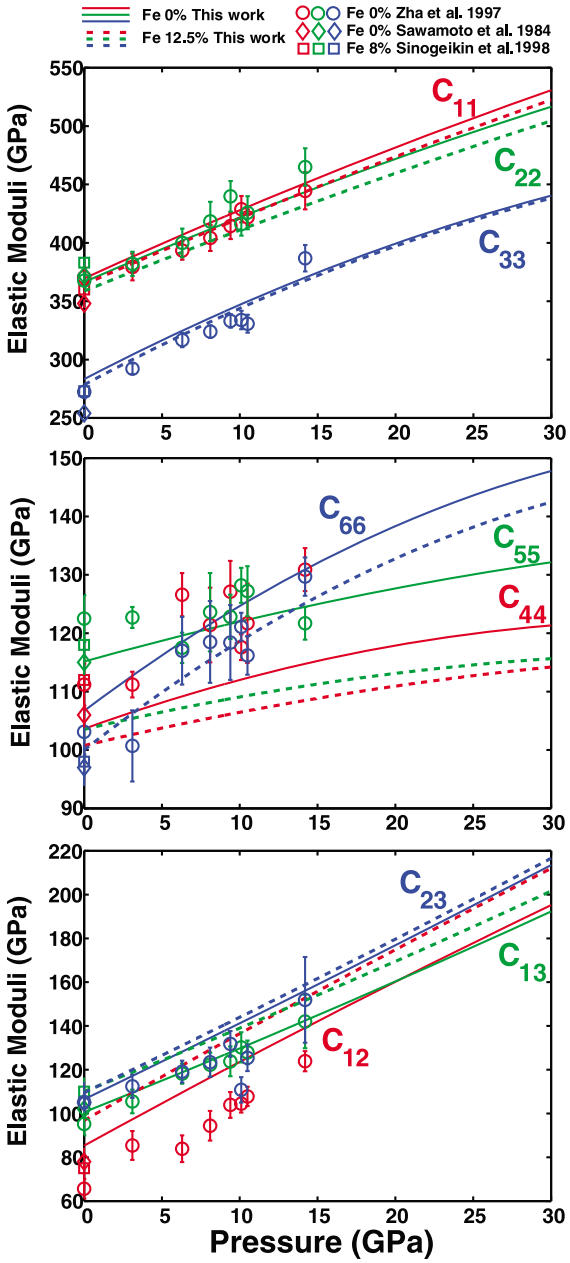

Figure 2. Cubic polynomial fits of static elastic constants of wadsleyite compared to experimental data at 300 K.

Inclusion of vibrational effects in the calculations should remove this discrepancy [*Wentzcovitch et al.*, 2010].

3.2. Elasticity of Wadsleyite and Ringwoodite

[11] Our predicted elastic constants of β–$(Mg_{1-x},Fe_x)_2SiO_4$ for $x = 0$ and $x = 0.125$ are shown in Table 2a and Figure 2. Available experimental data for $x = 0$ is quite scattered [*Zha et al.*, 1997], but they are in general agreement. As in olivine, C_{ij} with $i, j \leq 3$ increase monotonically and quasi-linearly with pressure, irrespective of iron content. In DFT-based results as in experiments, the shear elastic constants exhibit a nonlinear pressure dependence [*Núñez Valdez et al.*, 2010; *Zha et al.*, 1997]. The incorporation of iron produces a moderate decrease in C_{11}, C_{22}, and C_{33} of ~1–3%, with the latter being the least affected. The decrease is larger in shear C_{ij}, i.e., ~5% for C_{44} and C_{66}, and ~11% for C_{55}. On the other hand, off-diagonal C_{ij} increase between 1.4% and 14% with C_{12} and C_{23} showing the largest and smallest changes, respectively. At ambient conditions for $x = 0.08$ [*Sinogeikin et al.*, 1998], the increase–decrease pattern due to iron is shown experimentally as well, except in C_{22} and C_{23} for which the effect is unclear.

[12] The DFT-based C_{ij} of ringwoodite can be seen in Table 2b and Figure 3. Here the off-diagonal elastic constant C_{12} is the only one that shows an increase of ~4% when x changes from 0 to 0.125. C_{11} decreases by ~1.5% and C_{44} by ~6%. At ambient conditions, experiments do not offer a clear distinction between $x = 0$ [*Weidner et al.*, 1984] and $x = 0.09$ [*Sinogeikin et al.*, 2003].

[13] Table 3 and Figure 4 and Figure 5 show the pressure dependence of aggregate properties of wadsleyite and ringwoodite. Bulk (K) and shear (G) moduli shown in Figure 4a and Figure 5a are Voigt-Reuss-Hill averages [*Watt*, 1979; *Watt et al.*, 1976]. For the β–phase, by increasing x from 0 to 0.125, K increases ~1–2% in the 0–30 GPa pressure range, contrasting with G that decreases ~6%. For the γ–phase, K increases also ~1–2% while G decreases ~3–6%. Experimental trends also indicate that iron-free and iron-bearing ($x_\beta = 0$, 0.08, 0.12 and $x_\gamma = 0$, 0.09) samples yield an almost imperceptible variation in the bulk modulus, while the shear modulus drops appreciably with iron incorporation [*Zha et al.*, 1997; *Sinogeikin et al.*, 2003; *Li and Liebermann*, 2000; *Weidner et al.*, 1984; *Li*, 2003].

3.3. Influence of Iron in Sound Velocities and Anisotropy

[14] Isotropic compressional (V_P), shear (V_S), and bulk (V_Φ) velocities are given by

$$V_P = \sqrt{\frac{K + \frac{4}{3}G}{\rho}}, \quad V_S = \sqrt{\frac{G}{\rho}}, \quad V_\Phi = \sqrt{\frac{K}{\rho}}, \tag{2}$$

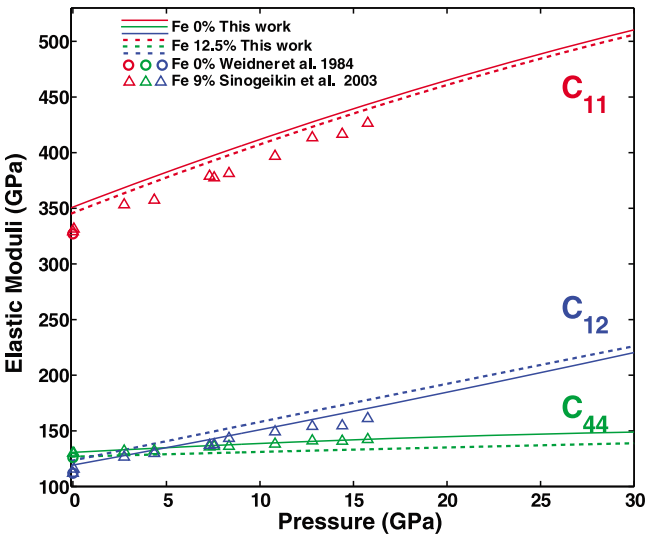

Figure 3. Cubic polynomial fits of static elastic constants of ringwoodite compared to experimental data at 300 K.

Table 3. Aggregate Properties Calculated at Zero Pressure of Olivine, Wadsleyite, and Ringwoodite

	α–$(Mg_{1-x},Fe_x)_2SiO_4$		β–$(Mg_{1-x},Fe_x)_2SiO_4$		γ–$(Mg_{1-x},Fe_x)_2SiO_4$	
Phase Fe %	0	12.5	0	12.5	0	12.5
K_0 (GPa)	136.8	139.0	177.6	180.4	196.5	197.1
G_0 (GPa)	83.3	79.4	112.9	106.0	124.7	120.5
$V_{P,0}$ (km/s)	8.7	8.4	9.6	9.4	10.0	9.7
$V_{S,0}$ (km/s)	5.0	4.8	5.7	5.4	5.9	5.6

where ρ is the density. They are shown in Figure 4b and Figure 5b and 0 GPa values are reported in Table 3. As expected, velocities of Fe-bearing phases are smaller than those of Fe-free phases due to the increase in density. Theoretical results are in excellent agreement with data obtained from Brillouin scattering and ultrasonic techniques [*Zha et al.*, 1997; *Li and Liebermann*, 2000; *Sinogeikin et al.*, 2003; *Weidner et al.*, 1984; *Li*, 2003; *Higo et al.*, 2006]. In the range of zero to 30 GPa, iron incorporation ($x = 0.125$) in wadsleyite decreases V_P, V_S, and V_Φ by ~2%, ~5%, ~0.5%, respectively. For ringwoodite the decrease in V_P is ~3%, in V_S is ~5%, and in V_Φ is ~1.5%.

[15] In interpreting seismic anisotropy in the transition zone, it is important to understand elastic anisotropy in wadsleyite and ringwoodite, its major constituents. We solve the Christoffel equation [*Landau and Lifshitz*, 1970] for acoustic velocities in single crystal:

$$\det\left|C_{ijkl}n_jn_l - \rho v^2\delta_{ik}\right| = 0, \tag{3}$$

where v is elastic wave velocity, **n** is propagation direction, δ_{ij} is Kronecker delta, and ρ is density. For a given **n**, there are three solutions, i.e., one P wave and two S waves (S1 and S2). The directional dependence of wadsleyite and ringwoodite P waves and S waves velocities for $0 \le x \le 0.125$ is shown in Figure 6 and Figure 7. For iron-free and iron-bearing β–phase, P wave velocities are qualitatively similar between 0 and 30 GPa, and they are extremal along [100] (fastest) and [001] (slowest) directions. Regarding S wave velocities, for S1 the minimum direction of propagation along [010] at 0 GPa changes to the [001] direction at 30 GPa. S2 velocities are alike between 0 and 30 GPa. For the γ–phase, the extremal P wave velocities occur along the [111] (fastest) and [100] (slowest) directions. At 30 GPa and $x = 0.125$, the slowest and fastest propagation directions are interchanged. Similarly, the iron-bearing S2 wave at 30 GPa interchanges the slowest for the fastest direction of

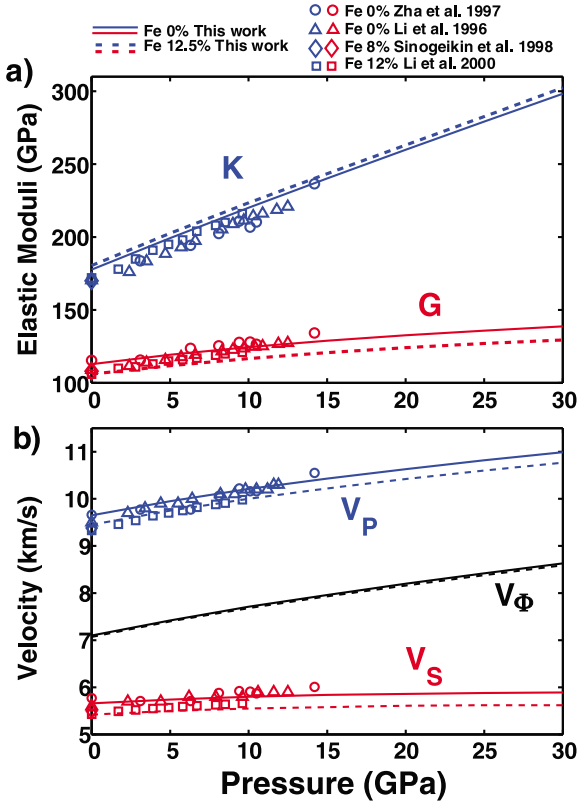

Figure 4. Pressure dependence of aggregate properties. (a) Voigt-Reuss-Hill average of bulk and shear moduli and (b) isotropic sound velocities of β–$(Mg_{1-x},Fe_x)_2SiO_4$ compared to experimental results.

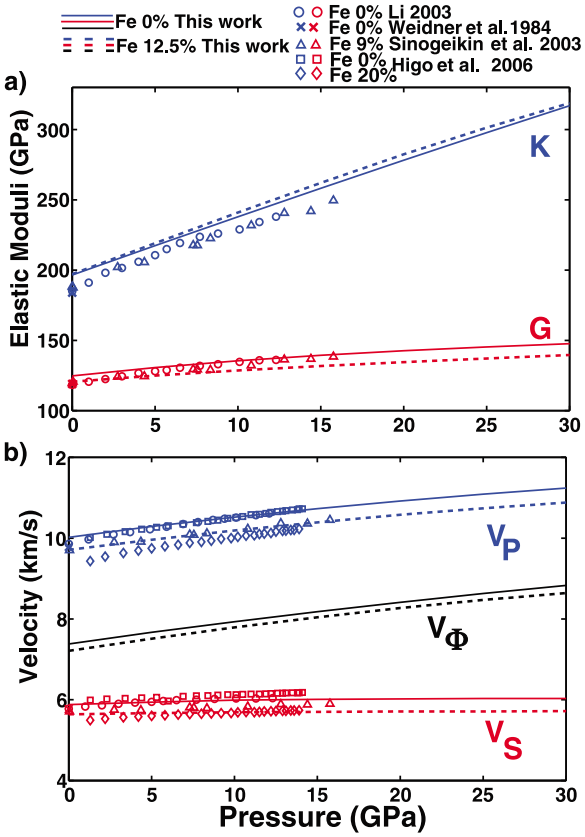

Figure 5. Pressure dependence of aggregate properties. (a) Voigt-Reuss-Hill average of bulk and shear moduli and (b) isotropic sound velocities of γ–$(Mg_{1-x},Fe_x)_2SiO_4$ compared to experimental results.

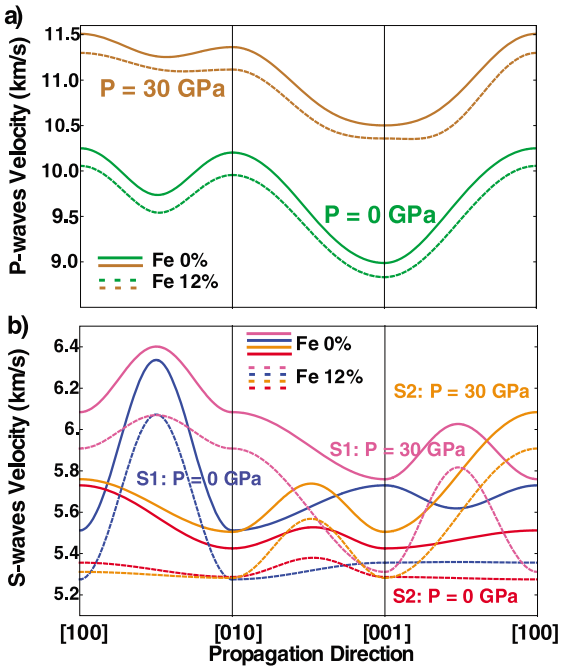

Figure 6. Variation of (a) compressional and (b) shear wave velocities of β–$(Mg_{1-x},Fe_x)_2SiO_4$ with propagation direction at 0 and 30 GPa.

propagation compared to the iron-free S2 wave. S1 waves propagation does not change qualitatively by varying x.

[16] Single crystal azimuthal anisotropy for compressional and shear waves (A_P and A_S, respectively), and polarization

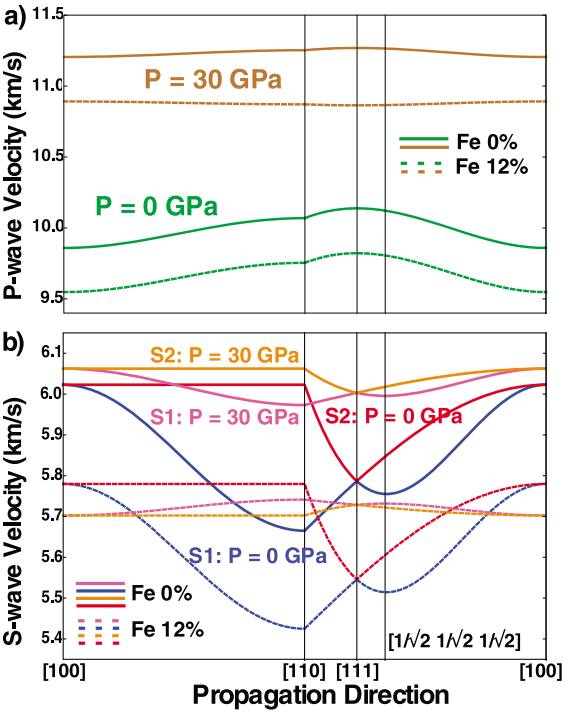

Figure 7. Pressure variation of (a) compressional and (b) shear wave velocities of γ–$(Mg_{1-x},Fe_x)_2SiO_4$ with propagation direction at 0 and 30 GPa.

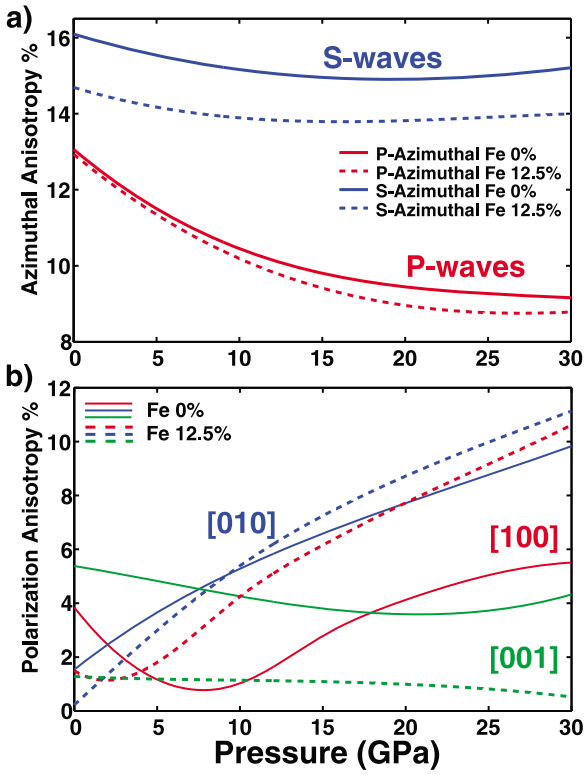

Figure 8. Pressure variation of (a) azimuthal and (b) polarization anisotropy in β–$(Mg_{1-x},Fe_x)_2SiO_4$.

anisotropy, $A^{pol}_{[ijk]}$, for shear waves (Figure 8 and Figure 9a), are quantified as

$$A_P = \left(\frac{v_{P\max} - v_{P\min}}{V_P}\right) \times 100, \quad (4)$$

$$A_S = \left(\frac{v_{S\max} - v_{S\min}}{V_S}\right) \times 100, \quad (5)$$

$$A^{pol}_{[ijk]} = \frac{|v_{S_1} - v_{S_2}|}{V_S} \times 100, \quad (6)$$

where V_P and V_S are aggregate velocities, and v_{S_1} and v_{S_2} are the two shear waves in the [ijk] direction. For cubic crystals, like ringwoodite, an anisotropic factor A, involving its three elastic constants, is defined as

$$A = \left(\frac{2C_{44} + C_{12}}{C_{11}} - 1\right) \times 100. \quad (7)$$

An elastically isotropic material has $A = 0$.

[17] Figure 8a shows that A_P for wadsleyite depends more strongly on pressure than A_S irrespective of x. A_P and A_S decrease with increasing x, but A_S is more sensitive. At pressures relevant to the transition zone, polarization anisotropy, Figure 8b, along [100] and [010] directions increases with iron content. In contrast, polarization anisotropy decreases in the [001] direction.

[18] Figure 9a shows A_P and A_S for ringwoodite. At ~27 GPa the iron-bearing phase becomes elastically isotropic, while the iron-free phase does not display such behavior.

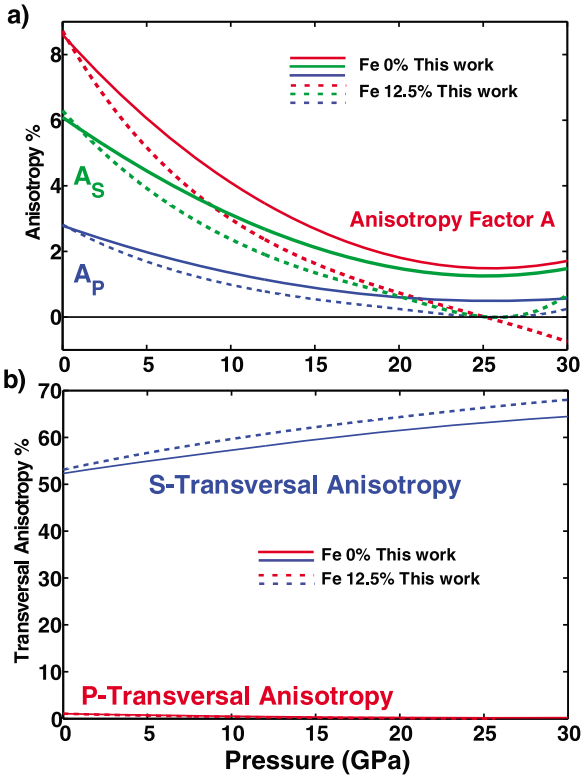

Figure 9. Pressure dependence of wave velocity anisotropy of γ–$(Mg_{1-x},Fe_x)_2SiO_4$ for (a) P waves and S waves (b) for a transversely isotropic aggregate.

[19] It is also important for seismology to study the anisotropy of transversely isotropic aggregates, which are characterized by five independent elastic moduli. For an aggregate with vertical symmetry axis in the [001] direction, these five parameters can be expressed in terms of single-crystal elastic constants as follows:

$$A = \frac{3}{8}(C_{11} + C_{22}) + \frac{1}{4}C_{12} + \frac{1}{2}C_{66}, \tag{8a}$$

$$C = C_{33}, \tag{8b}$$

$$F = \frac{1}{2}(C_{13} + C_{23}), \tag{8c}$$

$$N = \frac{1}{8}(C_{11} + C_{22}) - \frac{1}{4}C_{12} + \frac{1}{2}C_{66}, \tag{8d}$$

$$L = \frac{1}{2}(C_{44} + C_{55}). \tag{8e}$$

For symmetry axes along [100] and [010] directions, cyclic permutations of Cartesian indices can be used. Transverse anisotropies for longitudinal and shear waves are defined as

$$A_P^T = \left(\frac{v_{PH} - v_{PV}}{V_P}\right) \times 100 \quad \text{and} \qquad A_S^T = \left(\frac{v_{SH} - v_{SV}}{V_S}\right) \times 100, \tag{9}$$

respectively, where velocities are expressed in terms of parameters given in equation (8):

$$v_{PH} = \sqrt{\frac{A}{\rho}}, \quad \text{P–waves propagating horizontally,} \tag{10a}$$

$$v_{PV} = \sqrt{\frac{C}{\rho}}, \quad \text{P–waves propagating vertically,} \tag{10b}$$

$$v_{SH} = \sqrt{\frac{N}{\rho}}, \quad \text{S–waves polarized horizontally,} \tag{10c}$$

$$v_{SV} = \sqrt{\frac{L}{\rho}}, \quad \text{S–waves polarized vertically.} \tag{10d}$$

[20] Figure 10 shows transverse anisotropies for aggregates of wadsleyite with **a**, **b**, and **c** directions as axes of transverse isotropy. As a function of pressure and regardless of iron content, A_P^T slowly decreases in magnitude when the main crystallographic directions are vertically oriented. P waves always propagate faster when traveling parallel to [100] and [010] axes vertically oriented; thus anisotropy between 0 and 30 GPa is always negative. On the other hand, they travel more slowly along [001] when this is the vertical direction. Meanwhile, the transverse anisotropy of shear waves increases (decreases) in magnitude as pressure increases for **a** and **c** (**b**) preferred orientation axes. The

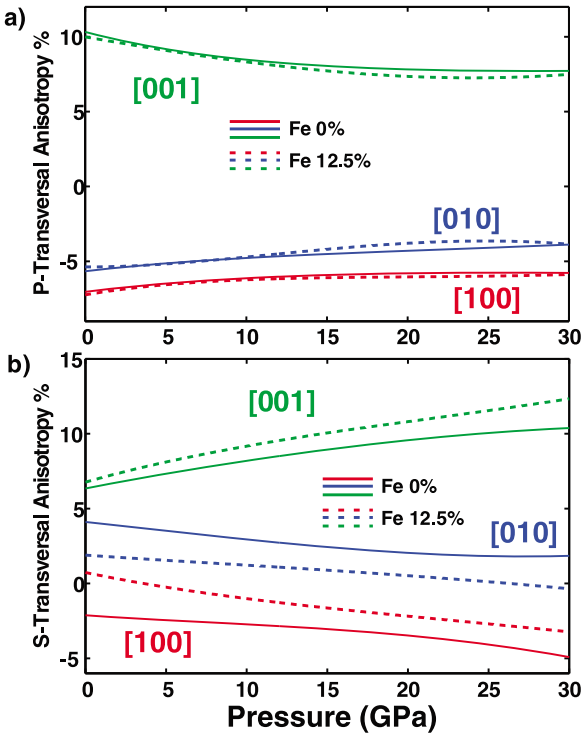

Figure 10. Pressure dependence of wave velocity anisotropy for a transversely isotropic aggregate of β–$(Mg_{1-x},Fe_x)_2SiO_4$ for (a) P waves and (b) S waves with a, b, and c crystallographic axes aligned in the vertical direction.

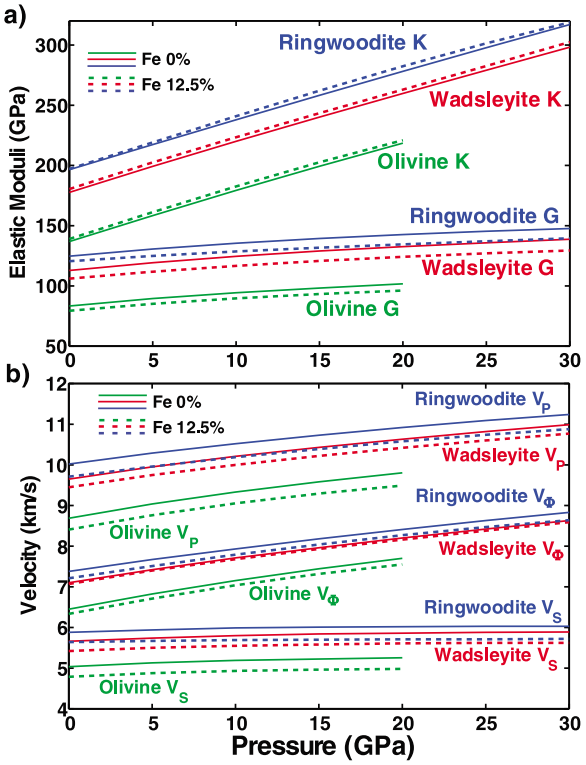

Figure 11. Comparison of aggregate properties of α–β–$\gamma(Mg_{1-x},Fe_x)_2SiO_4$. (a) Bulk and shear moduli and (b) sound velocities.

incorporation of iron increases A_S^T in the **c** direction and decreases it in the **a** and **b**.

[21] In ringwoodite, cylindrical geometry yields transverse anisotropy of shear waves increasing as a function of pressure and iron content. Increasing x from 0 to 0.125, A_S^T increases between 50% and 70%. In contrast, A_P^T is ~0% irrespective of iron (Figure 9b).

4. Geophysical Implications

[22] Upper mantle and transition zone discontinuities near 410 km and 520 km depth have been attributed to the $\alpha \rightarrow \beta$ and in part to $\beta \rightarrow \gamma$ phase changes. While the first is relatively sharp (~5 km wide) [*Agee*, 1998], the second has puzzled scientists for several reasons. For example, results from impedance studies [*Lawrence and Shearer*, 2006] suggest that the 520 km discontinuity must have in addition to the $\beta \rightarrow \gamma$ transition other significant sources like phase transitions in the pyroxene/garnet/Ca-perovskite system. Also, in the last decade there have been results indicating its geographically dependent splitting into two discontinuities: one at 500 km (possibly due to the $\beta \rightarrow \gamma$ transition) and another at 560 km (due to the Ca-perovskite exsolution from garnet perhaps) [*Saikia et al.*, 2008; *Deuss and Woodhouse*, 2001].

[23] On the other hand, the strong dependence of elastic moduli on iron content in minerals is well known, particularly in $(Mg_{1-x},Fe_x)_2SiO_4$. One could say that the elastic constants of olivine with variable iron content has been well characterized, experimentally and theoretically, at relevant pressures. This is not the case of wadsleyite and ringwoodite for which experiments barely reach transition zone conditions, making very difficult to establish definitive conclusions on the dependence of discontinuities caused by $\beta \rightarrow \gamma$ transitions on pressure, chemical composition, and temperature and its relationship with the 520 km discontinuity. This is the first study targeting pressure and chemical composition for β– and γ–phases at pressures of interest to the 520 km discontinuity, a step further toward the understanding of the effects of iron in the transition zone. In Figure 11 we summarize our first-principles results of aggregates of olivine, wadsleyite, and ringwoodite for the Mg end-members and for 12.5% of iron content as a function of pressure. In the following paragraphs we analyze changes in K, G, V_P, and V_S across these transformations as:

$$\Delta M = \frac{(M_{x,\chi} - M_{x,\xi})}{\frac{(M_{x,\chi}+M_{x,\xi})}{2}} \times 100, \qquad (11)$$

where M is a material's property in phases χ and ξ.

4.1. Results Related to 410 km and 520 km Discontinuities

[24] We examine elastic moduli and velocity contrasts for the $\alpha \rightarrow \beta$ transition between 10 to 15 GPa and for $\beta \rightarrow \gamma$ between 15 and 25 GPa (Table 4). These pressure ranges encompass the 410 km discontinuity at ~13.5 GPa and the controversial 520 km discontinuity at ~18 GPa. Our predictions suggest that across the $\alpha \rightarrow \beta$ transformation: ΔK is quite independent of iron content while ΔG is suppressed by the presence of iron. Regarding velocity contrasts, iron rises ΔV_P, ΔV_S, and ΔV_Φ in the interval 10–15 GPa. On the other hand, across the $\beta \rightarrow \gamma$ transition: ΔK is also almost independent of iron content, while ΔG is enhanced and ΔV_P, ΔV_S, and ΔV_Φ decrease with iron content between 15 and 25 GPa. Similar velocity contrasts were found by *Zha et al.* [1998] for the Mg–$\alpha \rightarrow \beta$ transition (~13.5 GPa) at ambient temperature. The effect of iron on ΔV_P and ΔV_S reported by *Sinogeikin et al.* [1998, 2003] is corroborated by our calculations only for the $\alpha \rightarrow \beta$ transformation but not for the $\beta \rightarrow \gamma$, for which we found opposite trends, that is, iron suppresses the contrasts. Other predictions indicate that temperature increases contrasts in bulk modulus and bulk velocity across the iron-free $\alpha \rightarrow \beta$ transition but has little effect across the the iron-free $\beta \rightarrow \gamma$ transition [*Yu et al.*, 2008]. Temperature effects in the presence of iron are beyond the scope of this paper and will be the subject of

Table 4. Theoretical Contrasts Across $\alpha \rightarrow \beta$ and $\beta \rightarrow \gamma$ Transitions

Transition	$\alpha \rightarrow \beta$		$\beta \rightarrow \gamma$	
Pressure range	10–15 GPa		15–25 GPa	
Fe %	0	12.5	0	12.5
ΔK^a %	20.4–18.6	20.1–18.3	7.3–6.5	7.4–6.5
ΔK^b %	~22	–	~7.2	–
ΔG^a %	27.6–27.1	26.1–25.7	7.8–6.8	8.7–7.6
$\Delta V_P{}^a$ %	9.0–8.5	10.0–9.5	2.8–2.5	1.7–1.3
$\Delta V_S{}^a$ %	~11.1	~11.8	2.9–2.5	2.1–1.6
$\Delta V_\Phi{}^a$ %	7.4–6.7	8.75–8.1	2.7–2.4	1.4–1.1
$\Delta V_\Phi{}^b$ %	~7.6	–	~2.7	–

[a]This work.
[b]*Yu et al.* [2008] with $\alpha \rightarrow \beta$ at ~1500 K and $\beta \rightarrow \gamma$ at ~1700 K.

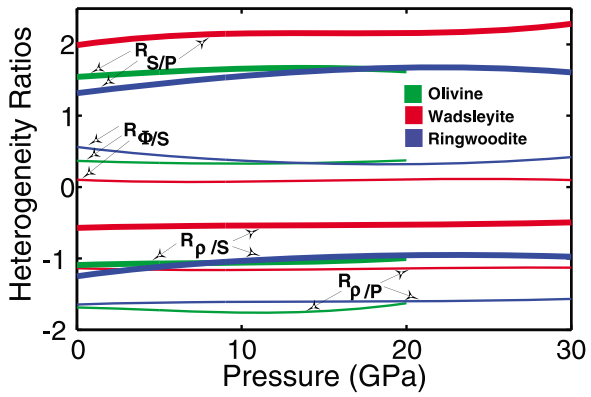

Figure 12. Heterogeneity ratios of α–β–$\gamma(Mg_{1-x},Fe_x)_2SiO_4$ caused by variation in iron concentration.

future work with the hope of clarifying the apparently contradictory results in the $\beta \rightarrow \gamma$ transformation.

4.2. Lateral Heterogeneity

[25] Lateral variations of velocity can originate from lateral variations of temperature, chemistry, or mineralogy. We quantify several heterogeneity ratios caused by lateral changes in iron content:

$$R_{S/P} = \frac{\delta \ln V_S}{\delta \ln V_P}, \quad R_{\Phi/S} = \frac{\delta \ln V_\Phi}{\delta \ln V_S}, \quad R_{\rho/P,S} = \frac{\delta \ln \rho}{\delta \ln V_{P,S}}. \quad (12)$$

In calculating these heterogeneity ratios, given the fact that we only have results for $x = 0$ and $x = 0.125$, we assume that velocities change linearly with x. This is a reasonable approximation due to the relatively small iron concentration. For large x this cannot be assumed. In Figure 12 one can see that for wadsleyite and ringwoodite $R_{S/P}$ varies between 1.3 and 2.3, while $R_{\Phi/S}$ varies between 0.05 and 0.6. These values are, within uncertainties, similar to results from tomographic studies compiled by *Karato and Karki* [2001]. $R_{S/P}$ is also comparable with that produced by lateral variations in temperature including the influence of phase transformations [*Stixrude and Lithgow-Bertelloni*, 2007]. On the other hand, $R_{\rho/P}$ and $R_{\rho/S}$ are negative for the three phases, in the range from −1.1 to −1.8 and from −0.5 to −1.3, respectively. Therefore $R_{\rho/S}$, $R_{\rho/P} < 0$ are good "fingerprints" of lateral variations of iron content. $R_{\rho/S}$, in contrast, is positive in the presence of lateral phase and/or temperature changes [*Stixrude and Lithgow-Bertelloni*, 2007; *Wentzcovitch et al.*, 2006]. Negative values for the upper mantle and transition zone summarized by *Karato and Karki* [2001] and suggested in the lower mantle by *Ishii and Tromp* [2001] could have contributions from lateral variations in iron (this was also noted by *Li* [2009]).

5. Conclusions

[26] We have used standard first-principles techniques to address the effect of iron on the elastic properties of wadsleyite and ringwoodite, β– and γ–$(Mg_{1-x},Fe_x)_2SiO_4$, the high-pressure polymorphs of olivine. In the pressure regime considered, 0–30 GPa, we found that static C_{ij} of γ–Mg_2SiO_4 agree better with available experimental data than β–Mg_2SiO_4 [*Weidner et al.*, 1984; *Zha et al.*, 1997; *Sinogeikin et al.*, 1998, 2003]. In wadsleyite C_{ij} with $i = j > 3$ are the most affected by iron, while in ringwoodite C_{44} is the most affected. We also found that the bulk modulus of both phases increases slightly upon iron substitution, and the shear modulus decreases, the latter being more significantly affected. These findings are consistent with trends suggested by experiments [*Li and Liebermann*, 2000; *Sinogeikin et al.*, 1998, 2003; *Higo et al.*, 2006]. We investigated in detail the elastic wave velocity anisotropy for single crystal and transversely isotropic aggregates of wadsleyite and ringwoodite. Here β– and γ–$(Mg_{1-x},Fe_x)_2SiO_4$ phases exhibit stronger azimuthal anisotropy for S waves than for P waves with iron decreasing both but affecting more S waves. Polarization anisotropy for the β–phase in [100] and [001] directions and transversal anisotropy of S waves are also significantly affected by iron. For the γ–phase, S-transversal anisotropy is quite large, increasing even more upon iron incorporation, while P-transversal anisotropy is almost null. These results might help in interpreting seismic anisotropies in the upper mantle–transition zone, for which some studies have found anisotropies of less than 4% [*Montagner and Kennett*, 1996; *Fischer and Wiens*, 1996]. Calculated velocities of Fe-bearing isotropic aggregates of wadsleyite and ringwoodite were found to be in excellent agreement with available data (<~14 GPa) from Brillouin and ultrasonic techniques [*Sinogeikin et al.*, 1998; *Li and Liebermann*, 2000; *Sinogeikin et al.*, 2003; *Higo et al.*, 2006]. Our static results indicate that iron enhances ΔV_P and ΔV_S across the $\alpha \rightarrow \beta$ transition, but suppresses them across the $\beta \rightarrow \gamma$ transition (Table 4). These findings are partially consistent with velocity contrasts obtained from ambient conditions measurements [*Sinogeikin et al.*, 1998, 2003]. Regarding heterogeneity ratios, we have presented a clear signature of lateral variation of iron content: $R_{\rho/S}$, $R_{\rho/P} < 0$. Overall, the importance of this work is to help clarify the effect of iron on the elasticity of α–β–γ–phases of the upper mantle and transition zone. Though our study is limited to static calculations, it seems that temperature will change the magnitude of elastic properties but not the general trends found here. Water must also play an important role in the properties of the transition zone minerals. Despite the progress made, further high-temperature studies, including water in addition to iron, are needed to improve interpretation of seismic observation of the upper mantle-transition zone.

[27] **Acknowledgments.** Research supported by the NSF/EAR-1019853, and EAR-0810272. Computations were performed at the Minnesota Supercomputing Institute and the Laboratory for Computational Science and Engineering.

References

Agee, C. B. (1998), Phase transformations and seismic structure in the upper mantle and transition zone, in *Ultrahigh-Pressure Mineralogy: Physics and Chemistry of the Earth's Deep Interior*, vol. 37, *Rev. in Mineral.*, edited by R. J. Hemley, pp. 165–203, Mineral. Soc. of Am., Washington, D. C.

Bass, J. D., S. V. Sinogeikin, and B. Li (2008), Elastic properties of minerals: A key for understanding the composition and temperature of Earth's interior, *Elements*, *4*, 165–170.

Caracas, R., and R. E. Cohen (2008), Ferrous iron in post-perovskite from first-principles calculations, *Phys. Earth Planet. Inter.*, *168*, 147–152.

Ceperley, D. M., and B. J. Alder (1980), Ground state of the electron gas by a stochastic method, *Phys. Rev. Lett.*, *45*, 566–569.

da Silveira, P., C. R. S. da Silva, and R. M. Wentzcovitch (2008), Metadata management for distributed first principles calculations in VLab–A collaborative cyberinfrastructure for materials computation, *Comp. Phys. Comm.*, *178*, 186–198.

Deuss, A., and J. Woodhouse (2001), Seismic observations of splitting of the mid-transition zone discontinuity in Earth's mantle, *Science*, *294*, 354–357.

Finger, L.W., R. M. Hazen, and T. Yagi (1979), Crystal structures and electron densities of nickel and iron silicate spinels at elevated temperature or pressure, *Am. Mineral.*, *64*, 1002–1009.

Finger, L.W., R. M. Hazen, J. Zhang, J. Ko, and A. Navrotsky (1993), The effect of Fe on the crystal structure of wadsleyite β–$(Mg_{1-x},Fe_x)_2SiO_4$, $0.00 \leq x \leq 0.40$, *Phys. Chem. Minerals*, *19*, 36–368.

Fischer, K. M., and D. A. Wiens (1996), The depth distribution of mantle anisotropy beneath the Tonga subduction zone, *Earth Planet. Sci. Lett.*, *142*, 253–260.

Giannozzi, P., et al.. (2009), QUANTUM ESPRESSO: A modular and open-source software project for quantum simulations of materials, *J. Phys. Condens. Matter*, *21*, 395502. [Available at http://www.quantum-espresso.org/]

Hazen, R. M., J. Zhang, and J. Ko (1990). Effects of Fe/Mg on the compressibility of synthetic wadsleyite: β–$(Mg_{1-x},Fe_x)_2SiO_4$ ($x \leq 0.25$), *Phys. Chem. Minerals*, *17*, 416–419.

Hazen, R. M., M. B. Weinberger, H. Yang, and C. T. Prewitt (2000), Comparative high-pressure crystal chemistry of wadsleyite, β–$(Mg_{1-x},Fe_x)_2SiO_4$, with $x = 0$ and 0.25, *Am. Mineral.*, *85*, 770–777.

Higo, Y., T. Inoue, B. Li, T. Irifune, and R. C. Liebermann (2006), The effect of iron on the elastic properties of ringwoodite at high pressure, *Phys. Earth Planet. Inter.*, *159*, 276–285.

Hohenberg, P., and W. Kohn (1964), Inhomogeneous electron gas, *Phys. Rev.*, *136*, B864–871.

Horiuchi, H., and H. Sawamoto (1981), β–$(Mg_{1-x},Fe_x)_2SiO_4$: Single crystal X-ray diffraction study, *Am. Mineral.*, *66*, 568–575.

Hsu, H., R. M. Wentzcovitch, K. Umemoto, and M. Cococcioni (2011), The Hubbard U correction and iron bearing minerals and the DFT + U functional, *Phys. Earth Planet. Inter.*, *185*, 13–19.

Irifune, T., and A.E. Ringwood (1987), Phase transformations in primitive MORB and pyrolite compositions to 25 GPa and some geophysical implications, in *High Pressure Research in Geophysics*, edited by M. Manghnani and Y. Syono, pp. 231–242, TERRAPUB, Tokyo.

Ishii, M., and J. Tromp (2001), Normal-mode and free-air gravity constraints on lateral variations in velocity and density of Earth's Mantle, *Science*, *285*, 1231–1236.

Karato, S., and B. B. Karki (2001), Origin of lateral variation of seismic wave velocities and density in the deep mantle, *J. Geophys. Res.*, *106*, 21,771–21,783.

Karki, B. B., L. Stixrude, S.J. Clark, M. C. Warren, G. J. Ackland, and J. Crain (1997), Elastic properties of orthorhombic $MgSiO_3$ perovskite at lower mantle pressures, *Am. Mineral.*, *82*, 635–638.

Kiefer, B., L. Stixrude, R. M. Wentzcovitch (1997), Calculated elastic constants and anisotropy of Mg_2SiO_4 spinel at high pressure, *Geophys. Res. Lett.*, *24*(22), 2841–2844.

Kiefer, B., L. Stixrude, and R. M. Wentzcovitch (1999), Normal and inverse ringwoodite at high pressures, *Am. Mineral.*, *84*, 288–293.

Kiefer, B., L. Stixrude, J. Hafner, and G. Kresse (2001), Structure and elasticity of wadsleyite at high pressures, *Am. Mineral.*, *86*,1387–1395.

Kiefer, B., L. Stixrude, and R. M. Wentzcovitch (2002), Elasticity of $(Mg,Fe)SiO_3$-Perovskite at high pressures, *Geophys. Res. Lett.*, *29*(11), 1539, doi:10.1029/2002GL014683.

Kohn, W., and L. J. Sham (1965). Self-consistent equations including exchange and correlation effects, *Phys. Rev. A*, *140*, 1133–1138.

Landau, L. D., and E. M. Lifshitz (1970), *Theory of Elasticity*, pp. 106–109, Pergamon, Oxford, U.K.

Lawrence, J. F., and P. M. Shearer (2006), Constraining seismic velocity and density for the mantle transition zone with reflected and transmitted waveforms, *Geochem. Geophys. Geosyst.*, *7*, Q10012, doi:10.1029/2006GC001339.

Li, B. (2003), Compressional and shear velocities of ringwoodite γ–(Mg_2SiO_4 to 12 GPa, *Am. Mineral.*, *88*, 1312–1317.

Li, B. (2009), Characteristics of lateral heterogeneities with thermal and chemical origins in the pyrolitic lower mantle, *Progr. Nat. Sci.*, *19*, 1603–16011.

Li, B., and R. C. Liebermann (2000), Sound velocities of wadsleyite β–$(Mg_{0.}88,Fe_{0.}12)_2SiO_4$ to 10 GPa, *Am. Mineral.*, *85*, 292–295.

Li, B., and R. C. Liebermann (2007), Indoor seismology by probing the Earth's interior by using sound velocity measurements at high pressures and temperatures, *Proc. Natl. Acad. Sci.*, *104*, 9145–9150.

Li, B., G. D. Gwanmesia, and R. C. Liebermann (1996), Sound velocities of olivine and beta polymorphs of (Mg_2SiO_4 at Earth's transition zone pressures, *Geophys. Res. Lett.*, *23*, 2259–2262.

Meng, Y., Y. Fei, D. J. Weidner, G. D. Gwanmesia, and J. Hu (1994), Hydrostatic compression of γ–(Mg_2SiO_4 to mantle pressures and 700 K: Thermal equation of state and related thermoelastic properties, *Phys. Chem. Minerals*, *21*, 407–412.

Montagner, J. P., and B. L. N. Kennett (1996), How to reconcile body-wave and normal-mode reference earth models, *Geophys. J. Int.*, *125*, 229–248.

Núñez Valdez, M., K. Umemoto, and R. M. Wentzcovitch (2010), Fundamentals of elasticity of $(Mg_{1-x},Fe_x)_2SiO_4$–olivine, *Geophys. Res. Lett.*, *37*, L14308, doi:10.1029/2010GL044205.

Panero, W. R. (2008), Cation disorder in ringwoodite and its effects on wave speeds in the Earth's transition zone, *J. Geophys. Res.*, *113*, B10204, doi:10.1029/2008JB005676.

Putnis, A. (1992), *Introduction to Mineral Sciences*, 399 pp., Cambridge Univ. Press, Cambridge, U.K.

Revenaugh, J., and T. H. Jordan (1991), Mantle layering from ScS reverberations: 2. The transition zone, *J. Geophys. Res.*, *96*, 19763–19780.

Rigden, S. M., G. D. Gwanmesia, J. D. Fitz Gerald, L. Jackson, and R. C. Liebermann (1991), Spinel elasticity and seismic structure of the transition zone of the mantle, *Nature*, *354*, 143–145.

Rinwood, A. E. (1975), *Composition and Petrology of the Earth's Mantle*, 618 pp., McGraw-Hill, New York.

Saikia, A., D. J. Frost, and D. C. Rubie (2008), Splitting of the 520-kilometer seismic discontinuity and chemical heterogeneity in the mantle, *Science*, *319*(5869), 1515–1518.

Sawamoto, H., D. J. Weidner, S. Sasaki, and M. Kumazawa (1984). Single-crystal elastic properties of the modified spinel (beta) phase of magnesium orthosilicate, *Science*, *224*(4650), 749–751.

Sinogeikin, S. V., T. Katsura, and J. D. Bass (1998), Sound velocities and elastic properties of Fe-bearing wadsleyite and ringwoodite, *J. Geophys. Res.*, *103*(B9), 20819–20825.

Sinogeikin, S. V., J. D. Bass, and T. Katsura (2003), Single-crystal elasticity of ringwoodite to high pressures and high temperatures: Implications for 520 km seismic discontinuity, *Phys. Earth Planet. Inter.*, *136*, 41–66.

Stixrude, L., and C. Lithgow-Bertelloni (2007), Influence of phase transformations on lateral heterogeneity and dynamics in Earth's mantle, *Earth Planet. Sci. Lett.*, *263*, 45–55.

Vanderbilt, D. (1990), Soft self-consistent pseudopotentials in a generalized eigenvalue formalism, *Phys. Rev. B*, *41*, R7892.

Wallace, D. C. (1972), *Thermodynamics of Crystals*, 20 pp., John Wiley, Hoboken, N. J.

Watt, J. P. (1979), Hashin-Shtrikman bounds on the effective elastic moduli of polycrystals with orthorhombic symmetry, *J. Appl. Phys.*, *50*, 6290–6295.

Watt, J. P., G. F. Davies, and R. J. O'Connell (1976), The elastic properties of composite materials, *Rev. Geophys.*, *50*, 6290–6295.

Weidner, D. J., H. Sawamoto, S. Sasaki, and M. Kumazawa (1984), Single-crystal elastic properties of the spinel phase of Mg_2SiO_4, *J. Geophys. Res.*, *89*(B9), 7852–7860.

Wentzcovitch, R. M. (1991), Invariant molecular dynamics approach to structural phase transitions, *Phys. Rev. B*, *44*, 2358–2361.

Wentzcovitch, R. M., J. L. Martins, and G. D. Price (1993), *Ab initio* molecular dynamics with variable cell shape: Application to $MgSiO_3$ perovskite, *Phys. Rev. Lett.*, *70*, 3947–3950.

Wentzcovitch, R. M., D. A. Hugh-Jones, R. J. Angel, and G. D. Price (1995), *Ab initio* study of $MgSiO_3$ C2/c enstatite, *Phys. Chem. Minerals*, *22*, 453–460.

Wentzcovitch, R. M., T. Tsuchiya, and J. Tsuchiya (2006), $MgSiO_3$–post perovskite at D″ conditions, *Proc. Natl. Acad. Sci. U. S. A.*, *103*, 543–546.

Wentzcovitch, R. M., Z. Wu, and P Carrier (2010), First priniciples quasi-harmonic thermoelasticity of mantle minerals, *Rev. Mineral. Geochem.*, *71*, 99–128.

Yu, Y., and R. M. Wentzcovitch (2006), Density functional study of vibrational and thermodynamic properties of ringwoodite, *J. Geophys. Res.*, *111*, B12202, doi:10.1029/2006JB004282.

Yu, Y., Z. Wu, and R. M. Wentzcovitch (2008), $\alpha \leftrightarrow \beta \leftrightarrow \gamma$ transformations in Mg_2SiO_4 in Earth's transition zone, *Earth Planet. Sci. Lett.*, *273*, 115–122.

Zha, C. S., T. S. Duffy, H. W. Mao, R. T. Downs, R. J. Hemley, and D. J. Weidner (1997), Single-crystal elasticity of β–Mg_2SiO_4 to the pressure of the 410 km seismic discontinuity in the earth's mantle, *Earth Planet. Sci. Lett.*, *147*, E9–E15.

Zha, C. S., T. S. Duffy, R. T. Downs, H. W. Mao, R. J. Hemley, and D. J. Weidner (1998), Single-crystal elasticity of the α and β Mg_2SiO_4 polymorphs at high pressure, in *Properties of Earth and Planetary Materials*

at High Pressure and Temperature, edited by M. H. Manghnani and T. Yagi, pp. 9–16, AGU, Washington, D. C.

P. da Silveira, Scientific Computation Program, University of Minnesota, Minneapolis, MN 55455, USA. (pedros@msi.umn.edu)

M. Núñez-Valdez, School of Physics and Astronomy, University of Minnesota, Minneapolis, MN 55455, USA. (valdez@physics.umn.edu)

R. M. Wentzcovitch, Department of Chemical Engineering and Materials Science, Minnesota Supercomputing Institute, University of Minnesota, Minneapolis, MN 55455, USA. (wentz002@umn.edu)